Influence of gas composition on wafer temperature in a tungsten chemical vapor deposition reactor: Experimental measurements, model development, and parameter identification

Hsiao-Yung Chang and Raymond A. Adomaitis[a)]
Department of Chemical Engineering and Institute for Systems Research, University of Maryland, College Park, Maryland 20742

John N. Kidder, Jr. and Gary W. Rubloff
Department of Material Science and Engineering and Institute for Systems Research, University of Maryland, College Park, Maryland 20742

(Received 13 April 2000; accepted 23 October 2000)

Experimental measurements of wafer temperature in a single-wafer, lamp-heated chemical vapor deposition system were used to study the wafer temperature response to gas composition. A physically based simulation procedure for the process gas and wafer temperature was developed in which a subset of parameter values were estimated using a nonlinear, iterative parameter identification method, producing a validated model with true predictive capabilities. With process heating lamp power held constant, wafer temperature variations of up to 160 K were observed by varying the feed gas H_2/N_2 ratio. Heat transfer between the wafer and susceptor was studied by shifting the instrumented wafer off the susceptor axis, exposing a portion of the wafer backside to the chamber floor. Model predictions and experimental observations both demonstrated that the gas velocity field had little influence on the observed wafer and predicted gas temperatures. © *2001 American Vacuum Society.* [DOI: 10.1116/1.1333076]

I. INTRODUCTION

Physically based process modeling and simulation methods have been gradually adopted as a design tool in the development of semiconductor manufacturing equipment. The value of process modeling is underscored by its broad acceptance[1–6] in the control systems designed to meet the more stringent requirements imposed by continually shrinking device sizes. The flexibility of simulation tools can be exploited to test the conceptual feasibility of new design ideas in early stages of equipment development, reduce process development cycles by prototyping system parameters in a process recipe, or give experimentally validated physical models that can be used for optimization of existing systems.

Many research studies have focused on modeling transport mechanisms in single wafer rapid thermal processing (RTP) systems,[7–11] where nonuniform heat transfer mechanisms can prevent across-wafer temperature uniformity during the process cycle. Typical modeling studies of RTP chemical vapor deposition (CVD) systems include a gas phase transport submodel and a wafer submodel to account for the interactions between the gas phase and wafer itself. In addition to the dominant radiative energy exchange modes inside the chamber, it is often found that conductive heat loss from the wafer to the adjacent gas phase is important in determining wafer temperature in low pressure reactors.[7,12–15] However, the influence of reactant gas composition on wafer temperature through gas thermal conduction has not yet been widely studied; this is partly attributable to the difficulty of quantifying the thermal conduction flux when a simplified boundary condition [e.g., terms such as $h(T_w - T_g)$] at the wafer/gas interface is used. Although a highly detailed, finely discretized gas phase transport submodel with special attention focused on the gas/wafer boundary condition solved simultaneously with the wafer dynamical submodel can provide insightful information on the gas conductive effect, the intensive computational requirements of this numerical solution procedure usually limits the applicability of such an approach. As an example, previous research by Hasper *et al.*[13] showed the gas conduction effect of pure hydrogen, argon, and a 50/50 hydrogen/argon mixture at different total pressures. Model predictions achieved very satisfactory agreement with experimental data for pure gases without parameter fitting, but the model predictivity was limited for gas mixtures because the lack of theoretical model parameter values for the gas mixtures.

In this article, we continue our work[16] of developing a low-order gas/wafer heat transfer model with true predictive capabilities. The model accounts for gas flow across the wafer, the three-dimensional gas temperature field, heat conduction within the wafer, and heat transfer between the wafer, gas, and reactor chamber. The gas temperature field submodel is solved using a global discretization method,[17,18] resulting in a relatively low order and computationally efficient simulation procedure. This model was used in an iterative, optimization-based parameter estimation procedure to determine a subset of the heat transfer parameters, using experimental measurements of wafer temperature as a function of gas composition. Additional experiments were conducted to show the minimal effect *total* gas flow rate had on observed wafer temperature when gas composition was held constant. This verified the model prediction of the dominance of gas

a)Author to whom correspondence should be addressed; electronic mail: adomaiti@isr.umd.edu

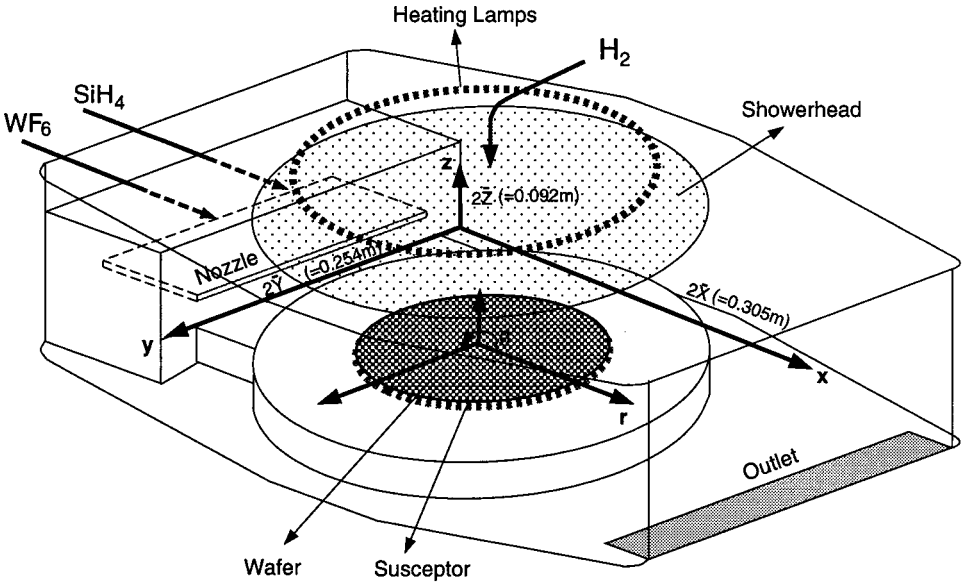

FIG. 1. Sketch of the tungsten CVD reactor system.

conductive heat transfer mechanisms relative to convective effects. What was produced was a validated process heat transfer model with relatively few adjustable parameters that gave valuable insight into the heat transfer mechanisms of this CVD system. The predictivity of this model can be used for developing a tighter temperature control system for this reactor[19] and for designing better conditioning procedures for process metrology.[20]

II. EXPERIMENT

Our research focuses on the ULVAC ERA-1000 selective tungsten deposition cluster tool, consisting of two single-wafer reactors joined by a buffer and a load-lock chamber for automatic loading and transfer of wafers. Figure 1 depicts the individual reactor configuration. Reactant gases are fed to the reactor from two sources: a gas mixture of silane and tungsten hexafluoride is injected through a two-dimensional nozzle installed on one side wall, and hydrogen is pumped in through a transparent showerhead mounted in the top of the reactor chamber. Gases mix in the chamber and react at the surface of a wafer located at the chamber center. Current experimental studies use 4 in. diameter wafers, although the tool is capable of processing 8 in. wafers. The wafer is supported by a slowly rotating 4 in. diameter quartz susceptor to assure the azimuthal symmetry of the deposited film. An incoherent tungsten–halogen lamp ring above and outside the reactor chamber is used to heat the wafer to 400 °C through the transparent quartz showerhead window. Typical deposition run times last 5 min after operating temperature is reached.

A SensArray 1530 thermocouple (TC) wafer was used to measure the true wafer temperature, and the system was operated in I/O mode to enable manual loading/unloading of the instrumented wafer. There are five thermocouples, labeled as shown in Fig. 2, attached to the top surface of this instrumented TC wafer. We note that the instrumented wafer is designed to measure the *wafer* temperature as opposed to wafer surface or thermocouple temperature by bonding the thermocouple leads in an undercut wafer area in a symmetric pattern.[21,22] A ± 1.0 °C or better measurement variation between these thermocouples has been reported.[21,22] The thermocouple wafer was intentionally shifted about 3.8 cm from susceptor center in the downstream direction, and slightly rotated so that thermocouple 5 was not located on top of the susceptor (see Fig. 2). This shifting was designed to study the conductive heat transfer from wafer to the underlying susceptor. The wafer rotation was turned off during the experiments to protect the leads of the test wafer.

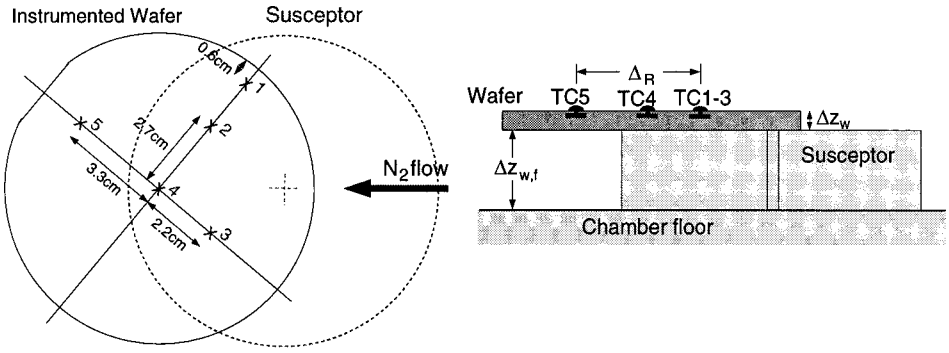

FIG. 2. Top and side views of the test wafer position with thermocouple positions marked.

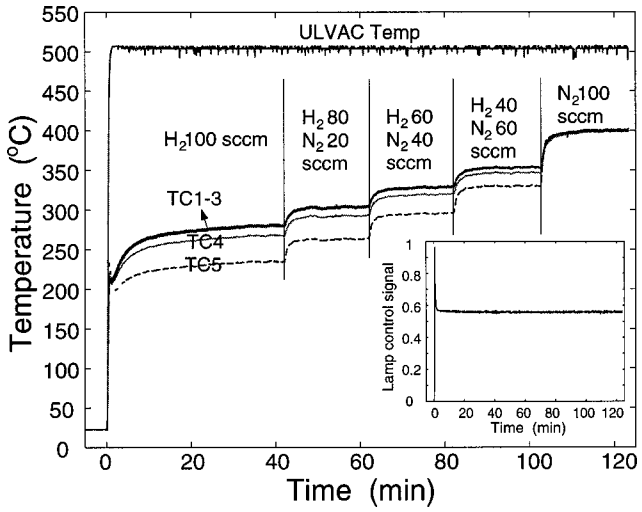

FIG. 3. Temperature response of the wafer to reactant gas composition variations.

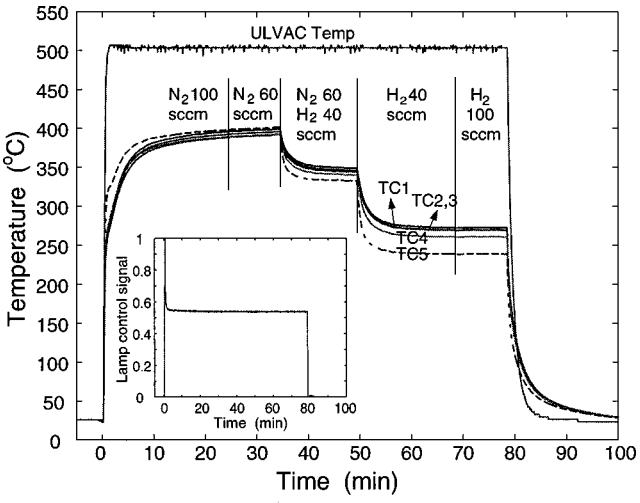

FIG. 4. Temperature response of the wafer to reactant gas flow rate and composition changes.

The temperature data collected from the instrumented wafer were sent to a personal computer based data acquisition system that included a LabView software interface and two computer boards: a CIO-DAS801 data acquisition board[23] and a CIO-EXP32 extension board.[24] Each thermocouple was connected to a channel on the expansion board, where a low pass filter with bandwidth 7 Hz was implemented between the high and low ends and a 100 kΩ resistor was installed between low and ground to provide ground reference. The temperature signals were then amplified 300-fold before being sent to the data acquisition board. An on-board semiconductor sensor provides the adjustable cold junction compensation (CJC) function that subsequently is used as a reference to the measured thermocouple signals in the LabView program. Additional processing variables of the ULVAC CVD system, such as the system thermocouple temperature measured near the lamp, lamp power control signal, chamber pressure, and gas feed rates, are collected during the processing cycle. The sampling rate selected was 20 Hz.

Two sets of experiments were conducted to investigate the influence of gas composition and total flow rate on wafer temperature in the ULVAC system. The first experiment, designed to study the effect of gas mixture composition at constant total flow rate, began by changing the initial reactant gases feed rates of 100 sccm pure hydrogen (case 1), to several different combinations: case 2: 80 sccm H_2/20 sccm N_2; case 3: 60 sccm H_2/40 sccm N_2; case 4: 40 sccm H_2/60 sccm N_2; and case 5: 100 sccm N_2. The gas flow rates/composition were changed only after the instrumented wafer temperature reached steady state in each period (approximately 20 min). The wafer temperature set point and chamber pressure were maintained at 500 °C and 500 mTorr throughout the experiments. The lamp power was observed to remain constant after the initial fast ramp-up despite the true wafer temperature variations attributable to the changes in gas composition, as shown in Fig. 3. This lack of movement of the system controller to compensate for true wafer temperature losses can be understood in terms of the following two reasons: first, the system thermocouple is located outside the reactor chamber, thus any gas composition change will have no effect on its temperature measurement; second, the fixed look-up table, designed to factor in the feed gas flows and chamber pressure when converting system thermocouple temperature to wafer temperature, was inactive in the I/O operation mode. Therefore, the system wafer temperature used as the feedback signal in the temperature control loop remained constant, producing no net set-point deviation. Detailed discussions regarding the ULVAC temperature control system can be found in Ref. 19.

The wafer temperature time histories for the first experiment are shown in Fig. 3. The wafer temperature indicated by the ULVAC control system (measured by the lamp thermocouple) is also plotted for reference. Generally, the steady-state wafer temperature was found to be lower in pure hydrogen than for pure nitrogen, and it gradually increased with nitrogen fraction. Because the lamp power output was maintained at a constant level, these temperature differences are due to the changing gas mixture properties, most importantly the gas thermal conductivity: we note that the pure hydrogen thermal conductivity is about six times larger than that of nitrogen at 500 mTorr. This gas property-related temperature difference is more significant in the measurement of TC No. 5, where the backside of the wafer contacts reactant gas instead of the quartz susceptor. The temperature deviation of TC No. 4 from TC Nos. 1–3 is due to the position of TC No. 4, which is close to the susceptor edge and is affected by the edge heat loss of the susceptor.

The second experiment was designed to study the effect of gas bulk velocity on wafer temperature, as well as to verify the observations made in the first experiment. In this experimental sequence, wafer heating was begun in pure nitrogen, and the compositional and total flow rates were changed according to case 1: 100 sccm N_2; case 2: 60 sccm N_2; case 3: 40 sccm H_2/60 sccm N_2; case 4: 40 sccm H_2; and case 5: 100 sccm H_2. The experimental results are plotted in Fig. 4. We note that when the wafer temperature responses

are compared for the different flow rates of cases 1 and 2 in pure nitrogen, as well as 4 and 5 in pure hydrogen, only insignificant differences were observed. This result indicates the gas convective heat transfer modeling terms can be neglected in the low pressure processing condition of the ULVAC system. Also, by comparing the temperature measurements of the second experiment to the first one at three different gas compositions (100 sccm N_2, 60 sccm N_2/40 sccm H_2, and 100 sccm H_2), the temperature differences are found to be less than 5 °C for pure nitrogen gas flow and are almost equal in the other two cases, demonstrating the repeatability of the experiments. In addition, it should be noted that the TC No. 5 measurement, represented as the dashed curve, responded faster during the initial heating ramp phase while the other thermocouples, positioned in the wafer area above the susceptor, showed slower temperature increases due to the additional energy absorbed by the underlying susceptor during the ramp-up phase.

III. MATHEMATICAL MODEL

An integrated model of the ULVAC tungsten CVD system has been developed that describes the interactions between gas phase velocity and temperature fields and the wafer thermal dynamics. The coordinates of gas phase and wafer computational domain are defined in Fig. 1. In the case of pure nitrogen flow, gas enters only through the side wall nozzle. For the operating conditions used in the experimented study, we should not expect turbulent or buoyancy-induced convective mixing effects;[16] therefore the gas will flow horizontally over the wafer for the pure nitrogen case (the case of nonzero hydrogen flow will be discussed later in the article). The fully developed, laminar velocity profile is described by the continuity and steady state Navier–Stokes equations

$$\frac{\partial v_x}{\partial x}=0, \tag{1}$$

$$\frac{\partial^2 v_x}{\partial y^2}+\alpha_v\frac{\partial^2 v_x}{\partial z^2}=\beta_v, \tag{2}$$

subject to no-slip boundary conditions at $y=0,1$ and $z=0,1$.

Because of the short residence time relative to wafer thermal dynamics, the gas temperature can be described by the steady-state conservation of energy

$$v_x\frac{\partial T_g}{\partial x}=\left(\delta_{gt}\frac{\partial^2}{\partial x^2}+\beta_{gt}\frac{\partial^2}{\partial y^2}+\gamma_{gt}\frac{\partial^2}{\partial z^2}\right)T_g=\mathcal{L}T_g. \tag{3}$$

Gas inlet temperature is assumed equal to the water-cooled chamber wall temperature; a zero gradient along flow direction boundary condition is used at the gas outlet. Gas temperature is set equal to showerhead and wafer temperature inside the relative areas at the top and bottom chamber surfaces. Overall, this gives the gas temperature boundary conditions:

TABLE I. Dimensionless parameters and variable definitions.

Dimensionless variables	Dimensionless parameters
$x=x^*/2\overline{X}$	$\alpha_v=\overline{Y^2}/\overline{Z^2}$
$y=y^*/2\overline{Y}$	$\beta_v=2\mathcal{P}\overline{Y^2}/(\mu\langle v\rangle\overline{X})$
$z=z^*/2\overline{Z}$	$\alpha_{gt}=\kappa/(\rho C_p)$
$v_x=v_x^*/\langle v\rangle$	$\delta_{gt}=\alpha_{gt}/(2\langle v\rangle\overline{X})$
$T_g=(T_g^*-T_{\text{amb}})/T_{\text{amb}}$	$\beta_{gt}=\alpha_{gt}\overline{X}/(2\langle v\rangle\overline{Y^2})$
	$\gamma_{gt}=\alpha_{gt}\overline{X}/(2\langle v\rangle\overline{Z^2})$
	$C_t=(T_{sh}^*-T_{\text{amb}})/T_{\text{amb}}$
	$C_b=(T_w^*-T_{\text{amb}})/T_{\text{amb}}$
	$R_{xy}=\overline{Y}/\overline{X}$
	$R_t=R_{sh}/2\overline{X}$
	$R_b=R_w/2\overline{X}$

$$T_g=0 \quad \text{at } x=0,$$

$$\frac{\partial T_g}{\partial x}=0 \quad \text{at } x=1,$$

$$T_g=0 \quad \text{at } y=0,1,$$

$$T_g=\begin{cases} C_t(T_{sh}^*) & \text{at } z=1, \quad (x-0.5)^2+R_{xy}^2(y-0.5)^2\leqslant R_t^2,\\ 0 & \text{at } z=1, \quad (x-0.5)^2+R_{xy}^2(y-0.5)^2>R_t^2,\end{cases}$$

$$T_g=\begin{cases} C_b(T_w^*) & \text{at } z=0, \quad (x-0.5)^2+R_{xy}^2(y-0.5)^2\leqslant R_b^2,\\ 0 & \text{at } z=0, \quad (x-0.5)^2+R_{xy}^2(y-0.5)^2>R_b^2.\end{cases} \tag{4}$$

The dimensionless parameters and variables are defined in Table I. The gas mixture density ρ, thermal conductivity κ, heat capacity C_p, and viscosity μ are determined from mixture-averaged properties[25] and the pure species viscosities are calculated from the kinetic theory of gases at the reference temperature $T_{\text{amb}}=298$ K (which is also the wall and inlet gas temperature). The values of $\overline{X}$, $\overline{Y}$, and $\overline{Z}$ are defined in Fig. 1; the wafer and showerhead radii are $R_w=0.0508$ m and $R_{sh}=0.1206$ m.

A. Wafer thermal dynamics model

The one-dimensional wafer thermal dynamics model can be written as follows:

$$\Delta_{z_w}\rho_w\frac{\partial(C_{pw}T_w)}{\partial t}=\Delta_{z_w}\kappa_w\nabla^2T_w+Q_{\text{lamp}}+Q_{\text{rad}}+Q_{\text{top}}+Q_{\text{bot}}, \tag{5}$$

where the energy fluxes from the lamp heating, radiation loss, convective/conductive losses from wafer top, and conduction loss from wafer bottom are defined as

$$
\begin{aligned}
Q_{\text{lamp}} &= \alpha_w(T_w) Q_{lp} u(t), \\
Q_{\text{rad}} &= -\frac{F_{A,\text{top}}\sigma(T_w^4 - T_{sh}^4)}{\epsilon_w^{-1}(T_w) + \epsilon_{sh}^{-1}(T_{sh}) - 1} \\
&\quad - \frac{F_{A,\text{bot}}\sigma(T_w^4 - T_f^4)}{\epsilon_w^{-1}(T_w) + \epsilon_f^{-1}(T_f) - 1}, \\
Q_{\text{top}} &= \kappa_g(T_{w,z=0}) \frac{\partial T_{g,z=0}}{\partial z}, \\
Q_{\text{bot}} &= -h_{\text{eff}}(T_w)(T_w - T_f).
\end{aligned}
\tag{6}
$$

In the model, the subscripts w, sh, and f represent the state variables or physical properties corresponding to the wafer, showerhead, and chamber floor, respectively. Δ_{Z_w} is the wafer thickness, σ is the Boltzmann constant, and F_A is the geometric factor that is equal to 1 for both wafer top and bottom surfaces.[26] h_{eff} is an effective heat transfer coefficient, Q_{lp} is the incident lamp bank emissive power at the wafer surface, and $u(t)$ is dimensionless time-dependent lamp control signal recorded from the experiments. ϵ is the temperature-dependent total emissivity interpolated from data points of silicon[27] and quartz[10] for the wafer and showerhead, respectively. A constant emissivity of 0.26 is used for the cooled, oxidized aluminum chamber wall and floor. The wafer absorptivity α_w is assumed equal to the emissivity of silicon.[28]

To describe the across-wafer temperature variations observed in our experimental data, we use different steady-state modeling approaches for wafer areas located above and beyond the susceptor outer edge. For the wafer region positioned above the susceptor (TC No.1-3), the governing Eq. (5) at steady-state becomes

$$
Q_{\text{lamp}} + Q_{\text{rad}} + Q_{\text{top}} + Q_{\text{bot}} = 0. \tag{7}
$$

The value of Q_{top} is computed by numerically differentiating the gas temperature at wafer/gas boundary as described in Eq. (6). Because the wafer is not clamped against the susceptor, there is no real solid-solid contact,[13] and therefore an effective heat transfer coefficient h_{eff} is used to approximate the combined heat transfer between wafer backside surface and chamber floor. This empirical, temperature-dependent heat transfer coefficient can be approximated by

$$
h_{\text{eff}}(T_w) = h_{\text{eff},0} + \alpha_0(T_w - T_{w,N_2}),
$$

which includes the nominal heat transfer coefficient $h_{\text{eff},0}$ and constant of proportionality α_0, that must be determined by fitting the experimental data to the model. Modeling the heat transfer in this form is equivalent to the Taylor's series expansion of the true function, evaluated at T_{w,N_2}. The wafer thermal conduction term $\Delta_{Z_w}\kappa_w\nabla^2 T_w$ is neglected because the averaged wafer temperature measurement from thermocouple Nos. 1–3 is used for data analysis. This conduction term proves to be small compared to other energy transfer mechanisms when estimated for the TC No. 5 location and we should expect an even smaller amount of energy to be conducted through the wafer in the region above the susceptor. Temperature data from thermocouple No. 4 is not considered here because it is affected by the susceptor edge heat transfer.

In the wafer region where thermocouple No. 5 is located, the wafer backside surface is in contact with reactant gas. The steady-state model takes the form

$$
Q_{\text{cond}} + Q_{\text{lamp}} + Q_{\text{rad}} + Q_{\text{top}} + Q_{\text{bot}} = 0. \tag{8}
$$

Q_{cond} is approximated using finite-difference formula

$$
Q_{\text{cond}} \approx \Delta_{Z_w}\kappa_w(T_{w,5}) \left(\frac{\overline{T}_{w,1-3} - T_{w,5}}{\Delta_R} - 0 \right) / \Delta_R,
$$

where Δ_R is the distance between thermocouple No. 5 and the averaged position of thermocouple Nos. 1–3.

Under low pressure processing conditions, the heat conduction between two parallel solid surfaces is proportional to the molecular mean free path in the gas phase. Because the gap distance between wafer and chamber floor is comparable to the gas molecular mean free path in the ULVAC system, the continuum flow model of the heat transfer must be modified and the correction of heat transfer coefficient is expressed as[13,14]

$$
h_{\text{eff}} \approx \frac{\kappa_g}{\Delta_{Z_{w,f}} + 2\beta_{w,f}\lambda}, \tag{9}
$$

where κ_g is the mean thermal conductivity evaluated at $\overline{T}_{w,f} = (T_w + T_f)/2$, $\Delta_{Z_{w,f}}$ is the wafer-floor gap distance, and λ is the mean free path defined by gas mixture molecular weight M, viscosity, and pressure p[25] as

$$
\lambda = 3.2\frac{\mu}{p}\left(\frac{R\overline{T}_{w,f}}{2\pi M}\right)^{1/2}.
$$

The constant $\beta_{w,f}$ is defined by thermal accommodation coefficient α and the ratio of specific heats $\gamma = C_p/C_v$ at constant pressure and volume:[13,14]

$$
\beta_{w,f} = \frac{2-\alpha}{\alpha}\frac{9\gamma - 5}{2\gamma + 2},
$$

and is on the order of unity.

B. Parameter estimation

There are several parameters in the wafer energy balance model for which values are difficult to compute accurately using published correlations or other *a priori* approaches. The lamp radiant flux intensity at the wafer surface, Q_{lp}, depends on the true emissive power of the heating lamps, the geometry of the reactor and chamber walls, and the adsorption characteristics of the quartz showerhead window. The upper limit of Q_{lp} of the ULVAC system, however, can be estimated by dividing the product of measured maximum lamp current and voltage by an approximated 0.3 m diameter circular area of the chamber floor.

The thermal accommodation coefficient α, used to define the constant $\beta_{w,f}$ in the conductive flux relation for the wafer/chamber floor gas gap, can deviate from the theoretical

TABLE II. Parameter values estimated from experimental data.

Variables	Guide values	Reference	Values identified in this study
Q_{lp}	46740 W/m^2	Maximum value	30341.6 W/m^2
$\beta_{w,f}$	≈ 1	Ref. 14 (theoretical value)	17.820
	30	Ref. 14 (estimated value)	
$h_{\text{eff},0}$	>0		3.409 W/(m^2 K)
α_0	$\alpha_0 < h_{\text{eff},0}/(120\text{ K})$		-0.048 W(m^2 K^2)

value calculated using the hard sphere molecular collision assumption.[13] Here we take the approach of Kleijn and Werner[14] to estimate the value of $\beta_{w,f}$ instead. As discussed in the previous section, the temperature dependent heat transfer coefficient h_{eff} must also be identified by using experimental measurements to accommodate the overall heat transfer coefficient that combines thermal conduction from wafer to susceptor, thermal conduction across the susceptor, and reactant gas thermal conduction between susceptor and chamber floor. The representative guide values of the system parameters to be estimated are listed in Table II for reference.

C. Solution procedure

To estimate the system parameters Q_{lp}, $\beta_{w,f}$, $h_{\text{eff},0}$, and α_0, we developed an iterative solution procedure that solves Eqs. (1)–(6) to resolve the interactions at the wafer/gas phase boundary. The overall solution algorithm begins by using the gas composition and measured wafer temperature to compute corresponding physical properties and to set the flow velocity and temperature field boundary conditions. The gas flow velocity field is computed using a Galerkin discretization technique[16] based on globally defined eigenfunctions; this solution approach determines the flow velocity component v_x and the pressure drop term β_v.

By defining the gas temperature as a linear combination of gas temperature inside the gas domain (T_Ω) and at the chamber top and bottom boundaries ($T_{\partial\Omega,t}, T_{\partial\Omega,b}$),

$$\begin{aligned} T_g &= T_\Omega + T_{\partial\Omega,t} + T_{\partial\Omega,b} \\ &= \sum_{l,m,n=1}^{L,M,N} b_{lmn}\phi_l(x)\psi_m(y)\zeta_n(z) \\ &\quad + \sum_{l,m=1}^{L,M} a_{lm}\phi_l(x)\psi_m(y)z \\ &\quad + \sum_{l,m=1}^{L,M} d_{lm}\phi_l(x)\psi_m(y)(1-z), \end{aligned} \tag{10}$$

we can formulate the residual of the gas temperature equation by substituting the corresponding trial function expansions into Eq. (3) to define the residual function

$$\mathcal{R} = \mathcal{L}T_\Omega + \mathcal{L}(T_{\partial\Omega,t} + T_{\partial\Omega,b}) - v_x\frac{\partial T_g}{\partial x}. \tag{11}$$

In Eq. (10) the b_{lmn}, a_{lm}, and d_{lm} are mode amplitude coefficients, and ϕ_l, ψ_m, and ζ_n are eigenfunctions in the three physical directions that satisfy $\mathcal{L}\phi\psi\zeta = \lambda\phi\psi\zeta$ and the homogeneous form of boundary conditions (4). The values of a_{lm} and d_{lm} are computed by projecting the gas temperature boundary conditions at $z=0,1$ onto $\phi_l\psi_m$. The residual function [Eq. (11)] is then projected onto the eigenfunctions using Galerkin's method. Because the eigenfunctions are defined by the eigenvalue problem $\mathcal{L}\phi\psi\zeta = \lambda\phi\psi\zeta$, we simplify the first term in Eq. (11) by replacing it with $\Sigma_{l,m,n=1}^{L,M,N}\lambda_{lmn}b_{lmn}\phi_l\psi_m\zeta_n$.

Because of the relatively minor contribution of the convective term $v_x\partial T_g/\partial x$, the mode amplitude coefficients can be determined by the convergent, iterative algorithm:

$$b_{i,j,k} = -\left\langle \mathcal{L}(T_{\partial\Omega,t} + T_{\partial\Omega,b}) - v_x\frac{\partial T_g}{\partial x}, \phi_i\psi_j\zeta_k \right\rangle \Big/ \lambda_{i,j,k}. \tag{12}$$

The weighted inner product is defined as

$$\langle f,g\rangle = \int_0^1\int_0^1\int_0^1 fg\,dx\,dy\,dz.$$

The representative gas temperature contours and wafer/gas energy transfer rate are displayed in Fig. 5 for the simulation condition corresponding 100 sccm N_2.

Taking the wafer-average gas/wafer heat transfer rate [Fig. 5(b)] as the Q_{top} in Eq. (6), we compute the wafer temperature using Newton's method to solve Eq. (7) for the TC Nos. 1–3 region and Eq. (8) for TC No. 5 region. The updated wafer temperature is then fed back to the gas temperature computation as a new boundary condition at the chamber floor, and the entire computation is performed again. This iterative wafer temperature computation scheme stops when a prespecified temperature error tolerance is satisfied.

The parameter estimation procedure is based on minimizing the sum of the squared errors (SSE), where the error is defined by the difference between the experimentally measured and predicted wafer temperature at each gas composition. A MATLAB optimization toolbox function `minsearch.m` is used for this parameter identification method. The total identification procedure consists of the two optimization substeps:

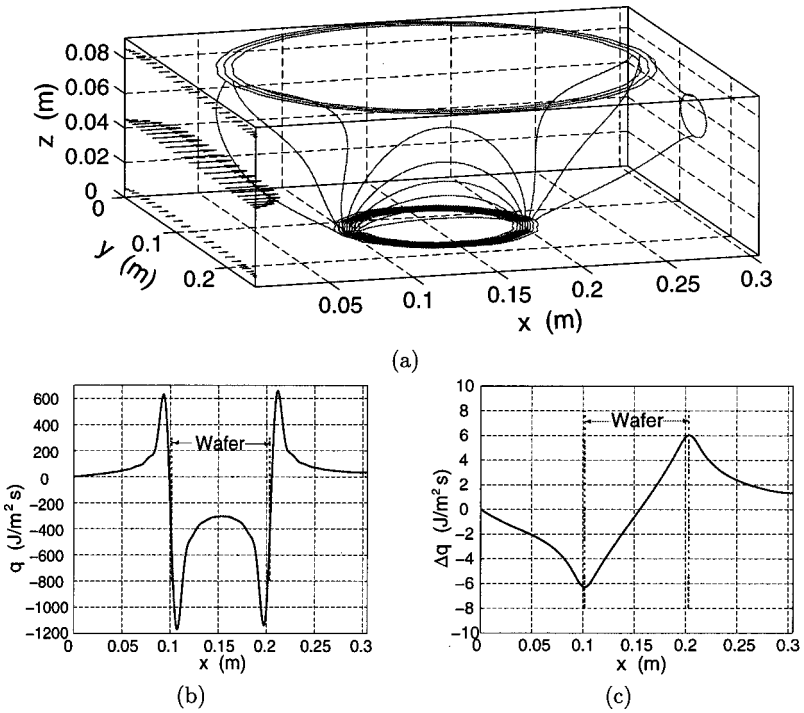

FIG. 5. (a) Gas flow field and temperature contours where each contour represents a 50 K temperature difference. (b) Wafer/gas heat transfer rate at reactor chamber centerline for $N_2=100$ sccm and 500 mTorr. (c) Difference of heat flux across wafer/gas boundary between $N_2=100$ and 60 sccm, where $\Delta q = q_{N_2=100} - q_{N_2=60}$.

(1) Estimate the values of Q_{lp} and $\beta_{w,f}$ by minimizing the objective function defined by temperature data from TC No. 5.
(2) Using the value of Q_{lp} estimated in the first step, calculate the effective heat transfer coefficient parameters $h_{\text{eff},0}$ and α_0 based on the minimizing the objective function defined by mean temperature measurement of TC Nos. 1–3.

The empirical showerhead temperature T_{sh} and floor temperature under the wafer T_f are assumed to be a constant 150 and 60 °C at steady state, respectively. These values were obtained after a number of parameter identification runs and are consistent with observations made during the experiments. Figure 6 shows the steady-state temperature measurements taken from Fig. 3; an extra wafer temperature point at 20% hydrogen was interpolated and used along with these measurements in the parameter estimation procedure. The estimated parameter values are listed in Table II.

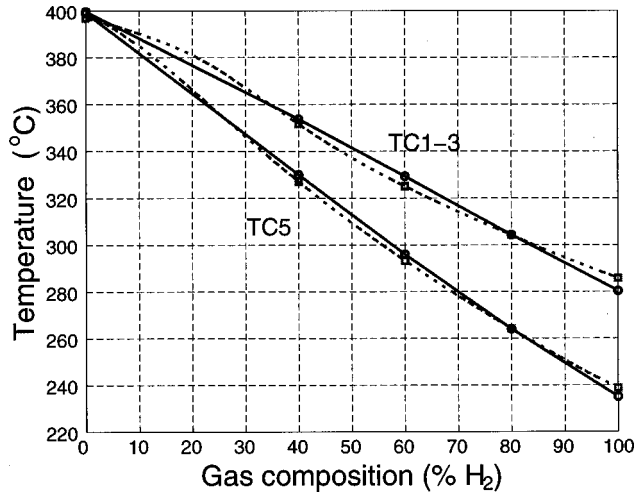

FIG. 6. Wafer temperature from experimental data (solid curves with circles at data points) and model prediction (dot–dash curves and squares).

IV. MODEL VALIDATION AND DISCUSSION

We approach the problem of assessing the validity of our CVD simulator from two directions. The first test consists of a direct comparison of the model predictions over the entire gas composition range to the interpolated experimental data curves. Because the observed wafer temperatures demonstrate a nearly linear correlation with gas H_2 fraction, this test provides a good indication of whether the model structure and parameter values correctly reflect the balance between the highly nonlinear contributions of radiative heat transfer terms and the composition-dependent heat transfer mechanisms. Comparing the model predictions and experimental data reveals a mean model prediction error of less than 3 K for each data set (Fig. 6). The heat transfer contributions from each term in Eq. (6) are plotted in Fig. 7. In both wafer regions, the radiative heat fluxes (Q_{lamp} and Q_{rad}) dominate in the high temperature range (>300 °C) and show nonlinear variations relative to the other heat transfer mechanisms because of the temperature dependency of wafer emissivity (absorptivity). The heat loss from Q_{bot}, which is more significant in the wafer area outside the susceptor [Fig. 7(b)], increases in higher hydrogen fractions due to increased gas thermal conductivity and becomes equivalent to Q_{rad} around 300 °C [corresponding to 80% H_2 in Fig. 7(a) and 60% H_2 in Fig. 7(b)]. The thermal conduction through the wafer resulting from wafer temperature nonuniformity is negligible

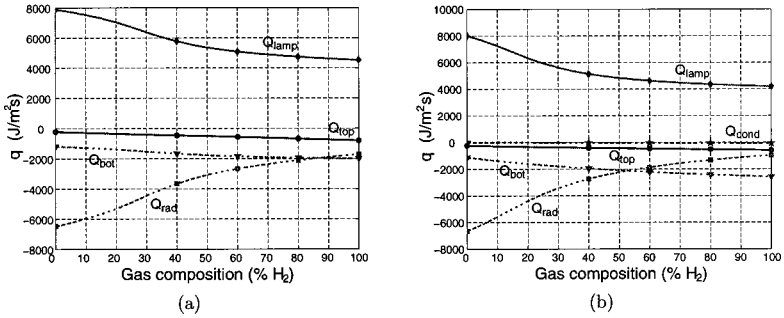

FIG. 7. Contributions of individual heat transfer mechanisms for the (a) interior region, and (b) region outside the susceptor.

[Fig. 7(b)], justifying the decision to ignore this term in the more temperature-uniform wafer interior region.

As the second test of model validity, we compare identified parameter values to values used in other studies, or compare our identified values to a range of values that can be theoretically justified. The guide and identified parameter values are compared in Table II. The system-dependent maximum incident lamp radiant flux Q_{lp}, identified using experimental data, is found to be about 65% of its maximum theoretical value. The constant parameter $\beta_{w,f}$, on the other hand, is an order of magnitude larger than the theoretical value, but it is close to the value identified by Kleijn and Werner[14] using data obtained from their low pressure CVD reactor. Finally, the overall wafer/chamber floor heat transfer coefficient must be positive. Because $T_w - T_{w,N_2} < 0$, the requirement $h_{\text{eff}} > 0$ translates into an upper limit of α_0 as defined in Table II; we note that the identified value satisfies this condition.

A. Solution insensitivity to flow field

In Fig. 5(c), we compare predicted gas/wafer heat transfer rates at 100 and 60 sccm nitrogen gas flows, corresponding to the experimental conditions used in Fig. 4. While these simulations are computed based on the averaged thermocouple temperature measurements of TC Nos. 1–3, similar results are obtained when TC No. 5 measurements are used in the computation. The differences of the energy flux across the wafer/gas boundary of both gas flow cases are less than 7 W/m^2 and are small compared to the magnitude of the gas heat transfer rate itself. These simulation results corroborate with our experimental observations that the convective heat transfer effects are negligible when compared to gas conduction. The combination of the model predictions and experimental observations of the relative insensitivity of the wafer temperature to the gas velocity field justifies our omission of detailed fluid flow simulations of the combined side inlet and showerhead inlet streams.

B. Extrapolation of model predictions

The validated model predictions can be directly or indirectly extrapolated to actual processing conditions. For example, because the convective heat transfer has only an insignificant effect on the wafer temperature, we can expect our wafer temperature predictions will not be affected by the 4 rpm wafer rotation used during process operation.

The use of the instrumented wafer limited experimental observations to tests only with nonreacting gas species. However, because wafer temperature was directly correlated to gas thermal conductivity in our modeling work, the results can be directly extrapolated to process gases containing WF_6 and H_2 and/or SiH_4 with adjustments made to wafer emissivity due to the deposited tungsten film. The model prediction of wafer temperature at the start of tungsten deposition process for various WF_6/H_2 gas compositions is shown in Fig. 8. Our current blanket tungsten deposition processing recipe[20] consists of 10 sccm WF_6 and 40 sccm H_2 with a 15–20 min preconditioning period; a wafer temperature of $T_w = 328\,^\circ\text{C}$ is predicted for the deposition period (compared to 500 °C from the ULVAC system reading).

V. CONCLUSIONS

The primary objective of this work was to study the influence of reactant gas composition on wafer temperature in a single-wafer CVD system. Both experimental observations and simulation studies showed the wafer temperature was a strong function of the wafer/gas interface thermal conduction compositional dependency; however, gas convective heat transfer mechanisms only had minimal effect on the wafer

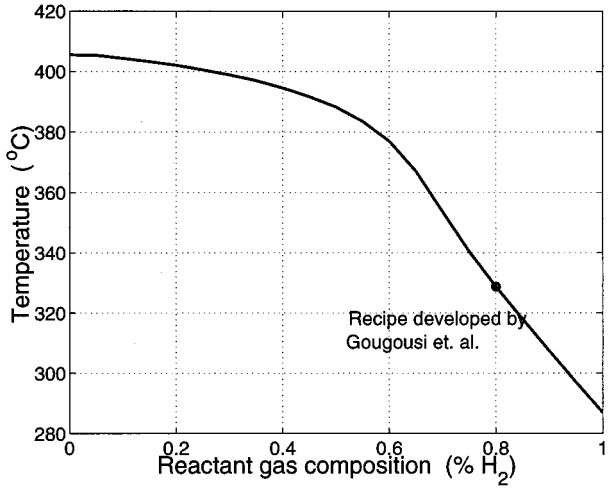

FIG. 8. Predicted wafer temperature at the beginning of tungsten deposition process plotted as a function of WF_6/H_2 gas composition at 0.5 Torr and 50 sccm total gas flow rate.

temperature. Good agreement was found between the model predictions and experimental data at various gas compositions, and the estimated parameter values were justified when compared with their guide values.

An important result of this experimental and simulation work was the validation of the theoretical predictions of previous modeling work.[16] In the cited paper, the minor contributions of convective gas phase transport mechanisms and gas phase nonlinearities (e.g., those important in higher-pressure systems, such as Refs. 29–31) were predicted for this low-pressure reactor system. Therefore, for the W CVD system studied in this work, a global spectral method approach was chosen over finite element and other localized discretization techniques. This choice was made to take advantage of the simplicity with which the global projection method could be implemented, allowing the researchers to focus on identifying the most important heat transfer modes in the system through an iterative parameter identification method.

ACKNOWLEDGMENTS

The authors wish to gratefully thank T. Gougousi, L. Henn-Lecordier, and Y. Xu for their technical support during the experimental work. H. Y. C. acknowledges partial support of the Small Smart Sensor Systems Center of the University of Maryland.

[1]B. Peuse, G. Miner, M. Yam, and C. Elia, Mater. Res. Soc. Symp. Proc. **525**, 71 (1998).
[2]P. Vandenabeele and W. Renken, Mater. Res. Soc. Symp. Proc. **525**, 109 (1998).
[3]K. Tsakalis and K. Stoddard, *Sixth IEEE International Conference on Emerging Technologies and Factory Automation*, pp. 514–519, 1997.
[4]T. S. Cale, P. E. Crouch, L. Song, and K. S. Tsakalis, *Proceedings of American Control Conference*, Seattle, WA, June 1995, pp. 1289–1293.
[5]C. D. Schaper, M. M. Moslehi, K. C. Sarawat, and T. Kailath, J. Electrochem. Soc. **141**, 3200 (1994).
[6]J. D. Stuber, I. Trachtenberg, T. F. Edgar, J. K. Elliott, and T. Breedijk, in *Proceedings of the 33rd Conference on Decision and Control*, Lake Buena Vista, FL, December 1994, pp. 79–85.
[7]H. A. Lord, IEEE Trans. Semicond. Manuf. **1**, 105 (1988).
[8]C. R. Kleijn, C. J. Hoogendoorn, A. Hasper, J. Holleman, and J. Middelhoek, J. Electrochem. Soc. **138**, 509 (1991).
[9]C. D. Schaper, Y. M. Cho, and T. Kailath, Appl. Phys. A: Solids Surf. **54**, 317 (1992).
[10]J.-M. Dilhac, N. Nolhier, C. Ganibal, and C. Zanchi, IEEE Trans. Semicond. Manuf. **8**, 432 (1995).
[11]C. D. Schaper and T. Kailath, J. Electrochem. Soc. **143**, 374 (1996).
[12]S. A. Campbell, K.-H. Ahn, K. L. Knutson, B. Y. H. Liu, and J. D. Leighton, IEEE Trans. Semicond. Manuf. **4**, 14 (1991).
[13]A. Hasper, J. E. J. Schmitz, J. Holleman, and J. F. Verwey, J. Vac. Sci. Technol. A **10**, 3193 (1992).
[14]C. R. Kleijn and C. Werner, *Modeling of Chemical Vapor Deposition of Tungsten Films* (Birkhauser, Boston, MA, 1993).
[15]C. R. Kleijn, edited by M. Meyyappan, *Computational Modeling in Semiconductor Processing* (Artech House, Boston, MA, 1995), Chap. 4.
[16]H.-Y. Chang and R. A. Adomaitis, Int. J. Heat Fluid Flow **20**, 74 (1999).
[17]Y. H. Lin, H.-Y. Chang, and R. A. Adomaitis, Comput. Chem. Eng. **23**, 1041 (1999).
[18]R. A. Adomaitis, Y. H. Lin, and H.-Y. Chang, Simulation **74**, 30 (2000).
[19]H.-Y. Chang and R. A. Adomaitis, AIChE Annual Meeting, Dallas, TX, 1999.
[20]T. Gougousi, Y. Xu, Jr., J. N. Kidder, G. W. Rubloff, and C. R. Tilford, J. Vac. Sci. Technol. B (submitted).
[21]P. Vandenabeele and W. Renken, Mater. Res. Soc. Symp. Proc. **470**, 181 (1997).
[22]P. Vandenabeele and W. Renken, Mater. Res. Soc. Symp. Proc. **470**, 17 (1997).
[23]Computer Boards, Mansfield, MA, *CIO-DAS801 and 802 User's Manual*, revision 1 edition, 1995.
[24]Computer Boards, Mansfield, MA, *CIO-EXP32/16 Hardware Manual*, revision 4 edition, 1994.
[25]R. J. Kee, G. Dixon-Lewis, J. Warnatz, M. E. Coltrin, and J. Miller, Technical Report SAND86-8246, Sandia National Laboratories, Albuquerque and Livermore, 1986.
[26]S. T. Hsu, *Engineering Heat Transfer* (Van Nostrand, Princeton, NJ, 1963).
[27]Properties of Silicon, United Kingdom, 1988.
[28]P. J. Timans, Solid State Technol. **37**, 63 (1997).
[29]H. K. Moffat and K. F. Jensen, J. Electrochem. Soc. **135**, 459 (1988).
[30]W. L. Holstein and J. L. Fitzjohn, J. Cryst. Growth **94**, 145 (1989).
[31]N. K. Ingle and T. J. Mountziaris, J. Fluid Mech. **277**, 249 (1994).